LAWRENCE
LIVERMORE
NATIONAL
LABORATORY

LLNL-PROC-425205

Propagation of Reactions in Thermally-damaged PBX-9501

J. W. Tringe, E. A. Glascoe, J. R. Kercher, T. M. Willey, H. K. Springer, D. W. Greenwood, J. D. Molitoris, L. Smilowitz, B. F. Henson, J. L. Maienschein

March 8, 2010

14th International Detonation Symposium
Coeur d'Alene, ID, United States
April 11, 2010 through April 16, 2010

Disclaimer

Propagation of reactions in thermally-damaged PBX-9501

Joseph W. Tringe*, Elizabeth A. Glascoe*, James R. Kercher*, Trevor M. Willey*, H. Keo Springer*, Daniel W. Greenwood*, John D. Molitoris*, Laura Smilowitz[f], Bryan F. Henson[f] and Jon L. Maienschein*

*Lawrence Livermore National Laboratory, Livermore, California, 94551

[f]Los Alamos National Laboratory, Los Alamos, New Mexico, 87545

Abstract. A thermally-initiated explosion in PBX-9501 (octahydro-1,3,5,7-tetranitro-1,3,5,7-tetrazocine) is observed *in situ* by flash x-ray imaging, and modeled with the LLNL multi-physics arbitrary-Lagrangian-Eulerian code ALE3D. The containment vessel deformation provides a useful estimate of the reaction pressure at the time of the explosion, which we calculate to be in the range 0.8-1.4 GPa. Closely-coupled ALE3D simulations of these experiments, utilizing the multi-phase convective burn model, provide detailed predictions of the reacted mass fraction and deflagration front acceleration. During the pre-initiation heating phase of these experiments, the solid HMX portion of the PBX-9501 undergoes a β-phase to δ-phase transition which damages the explosive and induces porosity. The multi-phase convective burn model results demonstrate that damaged particle size and pressure are critical for predicting reaction speed and violence. In the model, energetic parameters are taken from LLNL's thermochemical-kinetics code Cheetah and burn rate parameters from Son et al. (2000).[1] Model predictions of an accelerating deflagration front are in qualitative agreement with the experimental images assuming a mode particle diameter in the range 300-400 μm. There is uncertainty in the initial porosity caused by thermal damage of PBX-9501 and, thus, the effective surface area for burning. To better understand these structures, we employ x-ray computed tomography (XRCT) to examine the microstructure of PBX-9501 before and after thermal damage. Although lack of contrast between grains and binder prevents the determination of full grain size distribution in this material, there are many domains visible in thermally damaged PBX-9501 with diameters in the 300-400 μm range.

Introduction

PBX-9501 is an HMX-based explosive, nominally comprised of 94.9% HMX, 2.5% Estane, 2.5% nitroplasticizer, and 0.1% stabilizer. HMX undergoes a β-to-δ phase transition at about 162 C, which results in a minimum volume increase of 7%. However, PBX-9501 has been observed to expand up to 16% after unconfined heating at 180 C for just 30 minutes.[2] The additional volume is indicative of the significant microstructural changes that occur in this material. This damage likely plays an important role in the rapid convective burn process that has been observed with proton[3] and x-ray[4] radiography. In nominal self-combustion of intact energetic material (EM) at low pressure, the bulk of the energetic material is at a relatively cool temperature with a narrow heated, pyrolyzing zone at the surface[5]. The pyrolyzing surface zone releases intermediate gas products, which feed the flame in the gas phase. Heat is transferred from the reacting hot gas back to the surface mainly by

conduction. This process is often referred to as *conductive* burning (e.g., Berghout et al.)[6].

If the energetic material is not intact, but if there are fissures, cracks, fractures, pores, or packed fragments, then hot gas can penetrate into the non-intact volume of the energetic material, heat the exposed surface area, and eventually ignite the material over a potentially large area. Non-intact material could arise from mechanical damage due to impacts, thermal damage, strain from increasing gas pressure on deforming, confined energetic material, use of granulated material, etc. This process of penetration, heating, and ignition is often referred to as *convective* burning and has been reviewed extensively in the literature (e.g. Belyaev et al.[7], Bradley and Boggs[8], Bernecker[9], Asay et al.[10]). Convective burning is believed to be a precursor to deflagration-to-detonation transition (e.g., Belyaev et al.[7], Baer and Nunziato[11]). In the implementation of the convective burn model to be discussed here, we employ a direct calculation of the surface temperature of the EM particles, and employ a stability criterion for ignition instead of the more traditional heating-depth criterion.

Methods

Experimental

The PBX-9501 containment system for these experiments is comparable to those used in published studies employing proton radiography [3, 12, 13]. This system consists of two machined aluminum cylindrical cavities, assembled before the experiment to form a single sealed enclosure. The enclosure holds two pressed cylinders of PBX-9501, each 25.4 mm diameter and 12.7 mm tall. Cylinders are pressed to 96% of theoretical maximum density. Ullage near end caps allows for expansion of explosive during the β-to-δ phase transition. Resistive strip heaters are wrapped around the cylinders, controlled with signals from thermocouples positioned on the outside of the cylinders under the heater strips. Internal temperatures are monitored by a six-thermocouple array embedded at the interface between the assembled cylinders. In the experiment presented here, the containment system was also asymmetrically heated by lamps shining on one end cap of the cylinder.

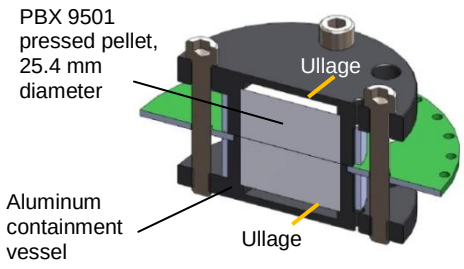

Fig. 1 Aluminum containment system for PBX 9501 pellets.

The assembled device is mounted in the Lawrence Livermore National Laboratory Hydra flash x-ray system as shown in Fig. 2. Hydra is a multiple-head x-ray system that has previously been used for observing dynamic phenomenon in various explosives and other materials [14, 15]. In this experiment, three of the x-ray images are obtained from nearly collinear viewing angles, while a fourth image is obtained from a perpendicular viewing angle.

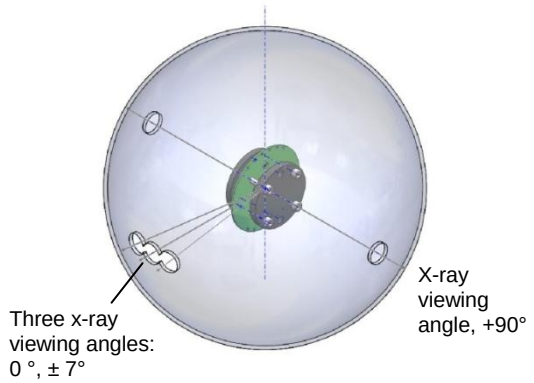

Fig. 2 X-ray imaging configuration for thermal explosion inside the firing tank; containment system not to scale.

The sample heating profile is similar to that reported in previous proton radiography studies of PBX 9501 thermal explosions: ramp at 5

C/minute to 70 C, hold for about 8 minutes, then ramp again at 5 C/minute to 178 C (above the 162 C HMX β-to-δ phase transition) and hold for 42 minutes. Finally, ramp at 5 C/min to 205 C and hold until the explosion self-initiates. Unlike previous experiments, where the thermal explosion is triggered with a laser pulse to ensure appropriate timing for imaging, these experiments do not employ an active trigger input. Instead, the same thermocouple array that monitors the internal explosive temperature also provides the trigger signal for the x-ray imaging system.

To examine the explosive morphology before and thermal damage, smaller PBX-9501 samples were prepared for computed tomographic (CT) imaging with synchrotron radiation. PBX-9501 was pressed into 0.125" (3.2 mm) diameter cylinders, about 0.25" (6.4 mm) tall. Similar to the larger pellets shown in in Fig. 1, pellets were pressed at 30,000 p.s.i. (2 x 10^8 Pa), 3 dwells of 3 minutes, each press, with the pressing die held at 85° C. Each of these samples weighed about 88-89 mg, with densities about 1.77 to 1.80 g/cm^{-3}, which is about 95.3 to 96.9% of the theoretical maximum density.

Six 6.4 mm tall and 3.2 mm-diameter pellets were thermally damaged for CT imaging. Pellets were heated inside closed, but unsealed, aluminum containers with ullage at top and bottom, volumetrically scaled from the 1" diameter pellet enclosures. Temperatures were measured by a thermocouple inside the enclosure. These samples were heated using infrared lamps for comparable times and temperatures as the 1" diameter parts shown in Fig. 1: ramp at 5 C/minute to 70 C, hold for about 8 minutes, then ramp again at 5 C/minute to 178 C and hold for 42 minutes. Two parts were heated just to the end of the 178 C temperature step. Two were further heated at 205 C for 3 minutes, and 2 were further heated at 205 C for 30 minutes - approximately the same duration at this step as was needed for the 1" diameter parts to begin to self heat. The measured temperature profile for these smaller parts corresponded to the temperature profiles of the 1" diameter parts, except that the smaller parts did not self-heat to a runaway condition.

The Lawrence Berkeley Laboratory Advanced Light Source (ALS) was used to obtain data for tomographic image reconstruction. ALS beamline 8.3.2, employed for these experiments, uses a superbend magnet source to attain energies up to 40 keV [16]. For these experiments, the multilayer monochromator was set to either 13 keV or 10.5 keV. The imaging system has a measured resolution of better than 4 μm; 1440 images were collected over 360 degrees at 3.6μm resolution, with bright-field images collected every 20 views. The tomographic slices were reconstructed via filtered backprojection using both the LLNL-developed ImageRec code and commercially available Octopus reconstruction code (University of Ghent, Belgium) to retrieve μ in units of mm^{-1} and/or cm^{-1} for each voxel within the volume.

Modeling

We have implemented a multi-phase convective burn model (MCBM) in ALE3D, a multi-physics, "arbitrary-Lagrangian-Eulerian finite element code that treats fluid and elastic-plastic response of materials on an unstructured grid"[17]. The MCBM is designed to interact with the chemistry module[18] of ALE3D and the multiphase module[19, 20], which maintains independent temperatures, (optionally) pressures, and velocities for each phase. The energetic material reactant can be intact or fragmented. If fragmented, the energetic material is described by a particle distribution specified by three bins. The current algorithm for MCBM provides for "convective burning" of fragmented energetic material and comprises four stages: convective heating of the particle surfaces, testing for ignition conditions being met, burning of the particles, and calculating the new particle size distributions at the end of the time step.

Experimental evidence has long established that there is a relation between pressure and pore diameter for ignition in pores or cracks of energetic materials [21-26]. We developed a new ignition criterion based on stability considerations of the flame-condensed-phase-energetic-material system. We derived the new criterion by perturbing solutions to a model of the flame-condensed-phase system, based on the model of Ward et al. [5] with the addition of an unsteady heat equation for the condensed phase. Our stability analysis suggests that for circumstances in

which the mass flux rate is highly sensitive to surface temperature, the critical pressure is related to the critical pore size by

$$P^{3n/2} d_p \geq c_1 \quad (1)$$

where the parameter c_1 is an explicit combination of heat capacities, conductance, density, and burn rate parameters.

We use the integral method of Goodman [27] to obtain an approximate differential equation for the temperature of the particle surfaces, as given by Eckert and Drake [28]. The heat transfer to the surface is based on empirical correlations of the Nusselt number compiled from the literature [29] [30-39] for fluidized and packed beds. The algorithm tests whether or not the surface of the particles has reached the ignition temperature and whether or not the pressure and hydraulic diameter satisfy Eq. 1. Both criteria must be met for ignition to occur.

Experimental results for dependence on pressure of laminar burning in energetic materials can usually be fit piecewise with expressions of the form aP^n where a and n are constants (Vieille's law or St. Robert's law). The theoretical model of Ward and co-workers [5] (hereinafter referred to as the WSB model) for HMX also fits the experimental pressure dependence well. Furthermore the WSB model also agrees with experimental results for the dependence of the burning rate on initial temperature of the energetic material.

If all particle size classes are burning, then the rate of decrease of the particle radius (burning rate) is the same for all size classes. However, because the smaller particles have greater area for equal volume fraction, those distributions made up of smaller particles have a greater rate of mass transfer from solid to gas phase than do those distributions with larger particles holding total volume fraction constant. At the end of each times-step, we update the volume-fraction distribution over the particle sizes to reflect the change in relative volumes due to burning during the time-step.

Results

Flash x-ray images of the explosion are shown in Fig. 3(a). The times indicated on the image correspond to the time elapsed since a 35 mV trigger signal from one of the embedded thermocouples, "TC 4" near the center of the 25.4 mm diameter cylindrical charge. The short-time thermocouple voltages are plotted as a function of time in Fig. 3(b), together with the output x-ray trigger voltage for reference. Note that these thermocouple voltages do not correspond to actual temperatures, as the sign of the voltage fluctuates. However, the signals are generally consistent among experiments in their absolute magnitude and, more importantly, with respect to their timing relative to the thermal explosion initiation process. In this experiment, some voltage begins to develop in all internal three thermocouples more than 10 μs before the trigger signal is initiated.

In addition to the internal thermocouples, thermocouples were placed outside the containment system, in proximity to the heating foil, and on the end cap thermocouple on the illuminated side. The "0 μs" flash x-ray image in Fig. 3(a) shows the thermal explosion initiating near the illuminated (and therefore preferentially heated) end cap. The deformation expands in the subsequent "10 μs" and "20 μs" images, and fast-camera record of the ruptured end cap at later time captured what is likely unreacted explosive bursting from edges (data not shown). Results from other similar experiments suggest that the velocity of this debris is about 2 km/s, slowing to 1 km/s within tens of μs of the end cap rupture.[4]

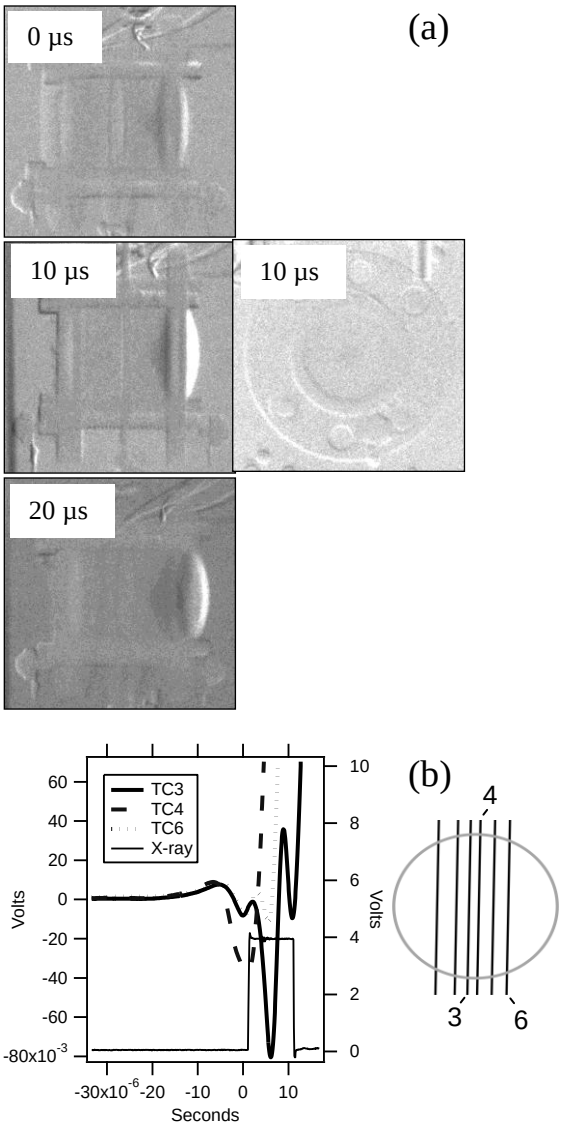

Fig. 3: (a) X-ray sequence showing side view of container, together with axial view at 10 µs (b) short-time thermocouple voltage history around the x-ray trigger time; top-down schematic of explosive at mid-plane, showing thermocouple positions.

The internal pressure which creates the end cap deformation shown in Figure 3(a) can be calculated with the known geometry and material properties of the containment cylinder. Note that the short times involved in this deformation event prevent de-pressurization of the cylinder along the centerline seam where the two halves of the container are joined (see Figure 1). In the quasi-plastic domain appropriate for the structure shown at 10 and 20 µs, the pressure, P (GPa), of a deflecting circular plate, fixed at the edges, can be described by

$$P = \frac{64 y_c E_t \, t^3}{a^4[12(1-\nu^2)]} \qquad (5)$$

where a is the end cap radius, t is the cap thickness, and y_c is the deflection, all in mm. ν is Poisson's ratio, taken to be 0.5. E_t is a tangent/plastic modulus, 0.65×E. E is Young's modulus, 207 GPa for our aluminum alloy. With this model, the pressure at 10 and 20 µs in Figure 3(a) corresponds to 1 and 1.4 GPa, respectively. Using a similar simple elastic model appropriate for the structure shown at 0 µs in Figure 3(a), an upper bound of 0.8 GPa can be established.

To simulate the post-ignition deflagration of a cylinder of PBX9501 with an initial diameter and length of 2.54 cm, confined in an aluminum case, which has been heated to 205˚C, we initialized the pressure to 254 bar corresponding to a density of approximately 0.07 g cm^{-3} of product gas. We assume that the ignition region is a disk 1.4 cm in diameter centered on the cylindrical axis next to end cap. To calculate heat transfer between the gas and the solid particles, we used the correlation for the Nusselt number for packed beds that was developed by Ranz [34] and recommended by Kunii and Levenspiel [40] and Gupta and Sathiyamoorthy [41]. The convective burn model was exercised for a range of particle sizes, with the mode diameter ranging from 100 microns to 1000 microns. The multiphase algorithm partitions the particle sizes into three size classes. We set the three sizes to be 0.5×mode, mode, and 1.02×mode with volume fractions of 0.05, 0.90, and 0.05, respectively. We set the mode to range from 100 to 1000 µm in either 50 or 100 µm increments. We initialized the total volume fraction of the solid phase particles to 0.92, which takes into account the fact that the volume fraction is reduced by thermal damage.

Figure 4 shows the density profile along the centerline of the cylinder in units of fraction of

charge length at 20 µsec from initialization. Note that the large particles show very little change in density whereas the smallest particle shows a density change well past the centerline of the cylinder.

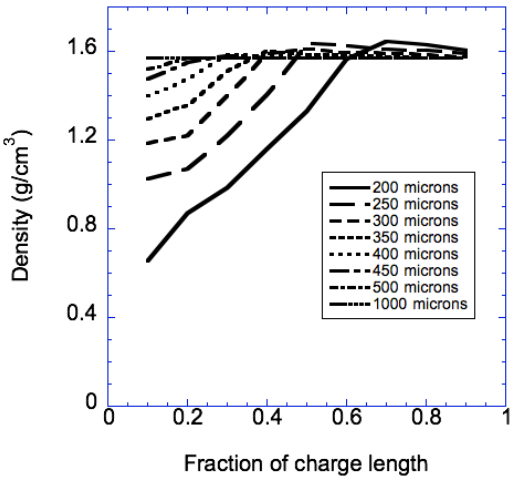

Fig. 4. Density in the cavity containing the thermally-damaged charge and product gases along the centerline of the cylinder at 20 µs. Initial ignition region was along the left-hand side of the figure.

In Fig. 5 we show time of "arrival" of various "fronts" along the centerline of the charge plotted against the distance along the centerline. We see that the temperature reaches 1000 K first, then 2000 K, followed shortly thereafter by ignition. About 10 µs later the density reaches 1.4 g/cm^3 followed after that by the density reaching 1.3 g/cm^3. Fig. 5 (a) is for 350 µm size particles, and Figure 5 (b) is for 400 µm particles.

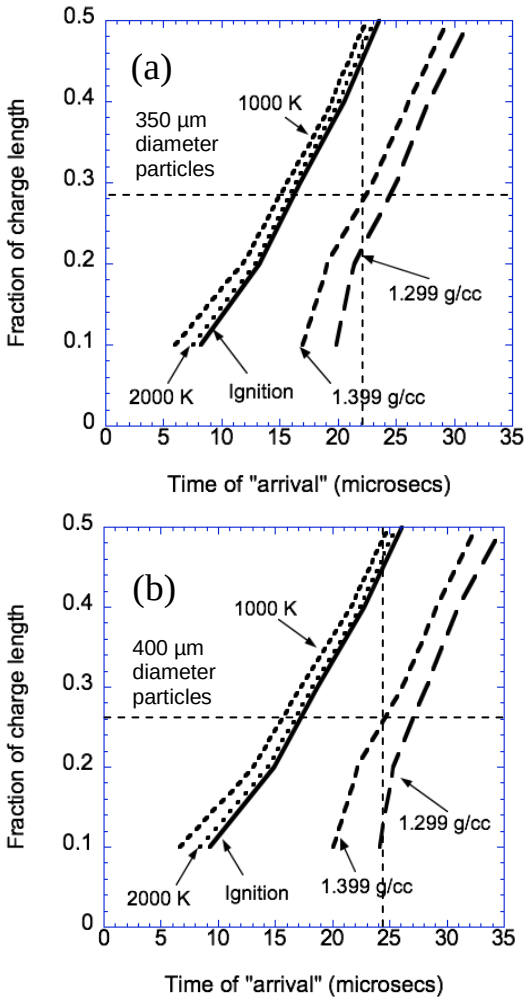

Fig. 5. The time and distance along the centerline for various variables reaching certain values 350 µm (a) and 400 µm (b) diameter particles.

A representative CT cross section of the top half of one of the most damaged 3.2-mm diameter pellets is shown in Fig. 5, together with an image of the same part before damage for comparison. The two slices are representative of central cross-sections in this pellet; the slices images have a resolution of 7.2 microns, while the images are averages of 8 slices (i.e. 58 microns thick). Superimposed on the damaged part is a circle with diameter 350 µm. Visible in both top and bottom slices are the cross-section HMX crystallites of a few hundred microns in diameter surrounded by slightly lower

density binder, as well as smaller voids tens of microns in diameter. The greatest change in the part before and after thermal treatment is the deformation of the top surface, which was relatively unconfined during heating. Multiple fissures appear near this surface. The HMX crystallites also appear to be generally smaller in the post heat-treatment slice, but the lack of contrast between grains and binder as well as fidelity in the reconstruction prevented the quantitative determination of full grain size distribution in this material before and after heating.

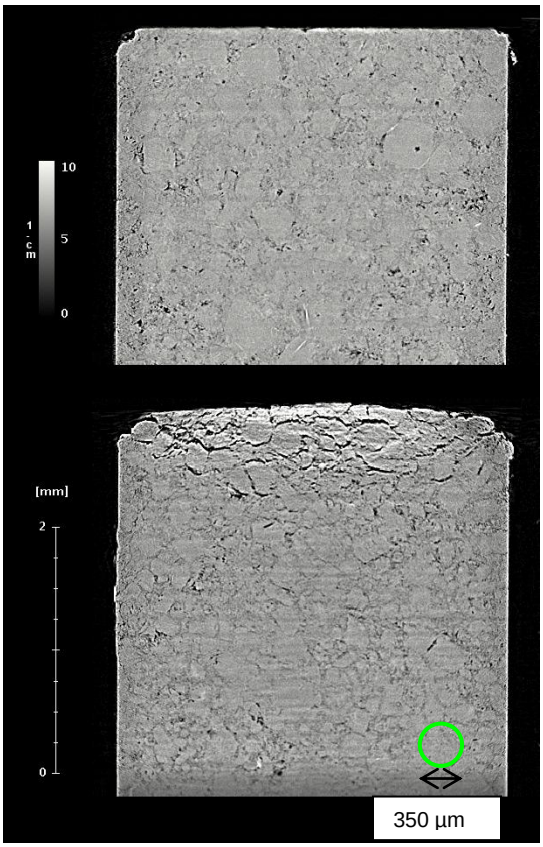

Fig. 5 Computed tomography cross section obtained with synchrotron radiation

Discussion

The flash x-ray images in Fig. 3(a) show a low-density (dark) domain expanding away from the apparent initiation location near the end cap. Based on previous proton and x-ray radiography data [4, 12], we hypothesize that the edge of this domain corresponds to the convective burn front. The two orthogonal images taken at the 10 µs indicate that the domain has an axis of symmetry coincident with the cylindrical axis of the PBX-9501 pellet. The fastest-moving surface of this domain is along the cylindrical axis of the pellet, moving away from the end cap. The end cap motion (appears bright at right in Fig. 3(a)) is much better-defined compared to the motion of the edge of the low-density domain. The instantaneous velocity of the center of the end cap between the 0 and 10 µs images is 90 m/s, while the velocity is 130 m/s between the 10 and 20 µs images. Based on the x-ray contrast in the three sequential side views in Fig. 3(a), the instantaneous velocity of the convective burn front may be up 1.5-2 times faster than the end cap velocity on average, placing it 6-8 mm (0.25-0.3 of the total charge length) from the original end cap location at 20 µs. These velocities are consistent with those previously observed by proton and x-ray radiography [4, 12].

The relationship between the flash x-ray image contrast and the actual density of the PBX-9501 is not presently well-defined. However, if the edge of the low-density domain corresponds to an average density of about 1.4 g/cm^2 (compared to ~1.8 g/cm^3 in the pre-damaged state), then the flash x-ray images are consistent with a mode particle size in the 300-350 µm range, as shown in Figs. 4 and 5. Smaller particles (e.g., 200 µm diameter) burn too quickly, while larger particles (500-100 µm diameter) burn too slowly, to be consistent with the observed x-ray contrast pattern. This 300-350 µm grain size range is plausible based on the cracks and domains present in the damaged PBX-9501 shown in Fig. 5. The 300-350 µm diameter particles are larger than the majority of the pristine PBX-9501 particles (85% of which are smaller than 150 µm in diameter), but may reflect an effective particle size for burning of damaged material.

The internal pressures that are calculated for these burn processes range from 0.1 GPa 12 µs after reaction initiation, to 1.6 GPa 39 µs after reaction initiation, in the case of 350 µm diameter particles. These pressures are generally consistent

with the 0.8-1.4 GPa pressures determined from the deformation of the aluminum end cap.

As noted previously, time "0" in the flash x-ray images Fig. 3(a) corresponds to the time at which the embedded thermocouples generate a pre-determined voltage threshold. Although the thermocouple signal does not map directly to temperature, nevertheless it could be generated by hot gasses passing over the embedded thermocouple junctions. This hypothesis is consistent with the ALE3D data presented in Fig. 5, where a 1000 K front of gas precedes the propagation of the lower-density domains by 10 μs or more. At the time the hot gas front (closely followed by ignition) passes over the center of the charge where the thermocouples are located, the density of the explosive in the vicinity of the thermocouples is essentially unchanged. In fact, the flash x-ray image at time "0" shows no change in density near the center of the charge.

Conclusions

We present flash x-ray images which show a likely convective burn front in a thermal explosion moving away from the initiation point at more than 100 m/s, tens of microseconds after initiation. A detailed particle-based model implemented in ALE3D predicts a hot gas front preceding the convective burn front, consistent with flash x-ray images and thermocouple data. The observed convective burn front velocities observed here and in other experiments [4, 12] indicate an effective particle diameter in the range 300-350 μm. Structures with this length scale are in fact present throughout damaged PBX-9501, as demonstrated by computed tomography (CT) images from data obtained by synchrotron radiation. The deformation of the aluminum enclosure suggests pressures in the range 0.8-1.4 GPa are present during the initial stages of the thermal explosion, consistent with our model's predictions.

Acknowledgements

This work performed under the auspices of the U.S. Department of Energy by Lawrence Livermore National Laboratory under Contract DE-AC52-07NA27344. Use of the Advanced Light Source is supported by the U. S. Department of Energy, Office of Science, Office of Basic Energy Sciences, under Contract DE-AC02-05CH11231.

References

[1] S. F. Son *et al.*, in Proceedings of the Combustion Institute 2000, pp. 919.
[2] J. T. Mang *et al.*, in *Shock Compression of Condensed Matter-2001, Pts 1 and 2, Proceedings*, edited by M. D. Furnish, N. N. Thadhani, and Y. Horie 2002, pp. 833.
[3] L. Smilowitz *et al.*, Physical Review Letters **100** (2008).
[4] J. W. Tringe *et al.*, in Conference of the American Physical Society Topical Group on Shock Compression of Condensed Matter, edited by M. Elert (American Physical Society, Nashville, TN, 2009).
[5] M. J. Ward, S. F. Son, and M. Q. Brewster, Combustion and Flame **114**, 556 (1998).
[6] H. L. Berghout *et al.*, Thermochimica Acta **384**, 261 (2002).
[7] A. F. Belyaev *et al.*, USSR Academy of Sciences-Institute of Chemical Physics. (1975).
[8] J. H.H. Bradley, and T. L. Boggs, (Naval Weapons Center, China Lake, CA, 1978).
[9] R. R. Bernecker, Aiaa Journal **24**, 82 (1986).
[10] B. W. Asay, S. F. Son, and J. B. Bdzil, International Journal of Multiphase Flow **22**, 923 (1996).
[11] M. R. Baer, and J. W. Nunziato, International Journal of Multiphase Flow **12**, 861 (1986).
[12] L. Smilowitz *et al.*, in Conference of the American-Physical-Society-Topical-Group on Shock Compression of Condensed Matter, edited by M. Elert *et al.*Waikoloa, HI, 2007), pp. 1139.
[13] L. Smilowitz *et al.*, Applied Physics Letters **90** (2007).
[14] P. C. Souers *et al.*, Propellants Explosives Pyrotechnics **31**, 89 (2006).
[15] J. W. Tringe *et al.*, in Conference of the American-Physical-Society-Topical-Group on Shock Compression of Condensed Matter, edited by M. Elert *et al.*Waikoloa, HI, 2007), pp. 1305.
[16] D. Robin *et al.*, Nuclear Instruments & Methods in Physics Research Section a-

Accelerators Spectrometers Detectors and Associated Equipment **538**, 65 (2005).
[17] A. Anderson *et al.*, edited by A. L. N. III (Lawrence Livermore National Laboratory Livermore, CA, 2009).
[18] A. L. Nichols, in Thirteenth International Detonation Symposium (Office of Naval Research 2007), pp. 1151.
[19] D. E. Stevens, M. J. Murphy, and T. A. Dunn, in Thirteenth International Detonation Symposium2007), pp. 1256.
[20] J. Knap *et al.*, (Lawrence Livermore National Laboratory, Livermore, CA, 2009).
[21] J. L. Prentice, (U.S. Naval Ordnance Test Station, China Lake, CA, 1962).
[22] L. Prentice, (China Lake Naval Weapons Center, China Lake, CA, 1977).
[23] T. Godai, AIAA Journal **8**, 1322 (1970).
[24] E. Andoh, and N. Kubota, Propellants and Explosives, 166 (1981).
[25] M. Kumar, S. M. Kovacic, and K. K. Kuo, Aiaa Journal **19**, 610 (1981).
[26] H. L. Berghout, S. F. Son, and B. W. Asay, Proceedings of the Combustion Institute **28**, 911 (2000).
[27] T. R. Goodman, Advances Heat Transfer **1**, 55 (1964).
[28] E. R. G. Eckert, and R. M. Drake, *Analysis of heat and mass transfer* (McGraw-Hill, 1972).
[29] V. Gnielinski, International Chemical Engineering **21**, 378 (1981).
[30] V. Gnielinski, in *Hemisphere Handbook of Heat Exchanger Design*, edited by G. E. Hewitt (Hemisphere Publishing Corp, 1990), pp. 2.5.4.
[31] D. Gunn, Intl. J. Heat Mass Transfer **21**, 467 (1978).
[32] W. M. Kays, and M. E. Crawford, *Convective heat and mass transfer* (McGraw-Hill, 1980).
[33] W. H. McAdams, *Heat transmission* (McGraw-Hill, 1954).
[34] W. E. Ranz, Chemical Engineering Progress **48**, 247 (1952).
[35] W. E. Ranz, and W. R. Marshall, Chemical Engineering Progress **48**, 141 (1952).
[36] W. E. Ranz, and W. R. Marshall, Chemical Engineering Progress **48**, 173 (1952).
[37] P. N. Rowe, and K. T. Claxton, Transactions of the Institute of Chemical Engineers **43**, T321 (1965).
[38] S. Whitaker, AIChE Journal **18**, 361 (1972).
[39] S. S. Zabrodsky, and H. Martin, in *Hemisphere Handbook of Heat Exchanger Design*, edited by G. E. Hewitt (Hemisphere Publishing Corp., 1990), pp. 2.5.5.
[40] D. Kunii, and O. Levenspiel, *Fluidization engineering* (Butterworth-Heinemann, Stoneham, MA, 1991).
[41] C. K. Gupta, and D. Sathiyamoorthy, *Fluid bed technology in materials processing* (CRC Press, Boca Raton, FL, 1999).